



Modeling of the mass transfer in continuous electrocoagulation process with bipolar electrodes

Jun Lu*, Zhenting Yang, Jin Chen, Kai Xu, Tongyi Yang, Jing Zhang

School of Environmental and Chemical Engineering, Jiangsu University of Science and Technology, Zhenjiang, Jiangsu 212003, China, emails: jluabc@163.com (J. Lu), 1060156271@qq.com (Z. Yang), 1135575953@qq.com (J. Chen), 947439595@qq.com (K. Xu), 490608791@qq.com (T. Yang), 82618354@qq.com (J. Zhang)

Received 28 May 2018; Accepted 4 November 2018

ABSTRACT

The continuous electrocoagulation (EC) with bipolar electrode was modeled and simulated. The generation and mass transfer of coagulants and hydroxide flocs were simulated. The electrocoagulation with bipolar electrode (B-EC) was compared with the electrocoagulation with monopolar electrode (M-EC). During B-EC, the flocs are uniformly generated and distributed in the channel. During M-EC, the flocs are generated in the extremely narrow area, which is located in the middle of EC channel. This concentration distribution is suitable for the formation of hydroxide flocs. Also another advantage should be mentioned is that the concentration of produced H^+ and OH^- is much lower in B-EC. The lower concentration of H^+ and OH^- is suitable for the formation of Al hydrate flocs. Thus, the bipolar electrode structure improves the mass transfer of generated coagulants, when compared with the monopolar electrode. Under the same total current, the B-EC has much higher flocs production than that of M-EC. The edge effects of bipolar electrode in B-EC were modeled and studied. The edge effects were discussed with the consideration of mass transfer. In the edge areas, the concentration of cation and anion hydroxide species is not negligible. The electro-migration in the direction perpendicular to the streamline will also make the ionic hydroxide species transfer into the bulk channel. Thus, in edge area, the electro-migration could also contribute to the mixture of the ions. The edge effect of bipolar electrode in EC process could be neglected.

Keywords: Electrocoagulation; Mass transfer; Bipolar electrode; Model; Simulation

1. Introduction

Electrocoagulation (EC) which is a kind of electrochemical wastewater treatment method is characterized by in-situ generation of coagulant and hydroxide flocs with high absorption ability. EC is an environmental friendly process for treating wastewater with heavy metal ions and toxic organics. During electrocoagulation (EC) process, the Al^{3+} (or Fe^{2+}) and OH^- , which are released from anode and cathode, will transfer into bulk solution by electro-migration and diffusion (Fig. 1). The electro-generated ions will undergo further spontaneous hydrolysis reactions to form hydroxide flocs [1]. These flocs have large surface areas, which are beneficial

for a rapid adsorption and pollutant trapping [2–6]. Thus, the generation and mass transfer of the electro-generated hydroxides and flocs will have important effect on pollutant removal [7–10].

Most of the recent research focused on the optimization and application of EC process for treating kinds of wastewater [11–13]. Response surface methodology was used to optimize the influence of experimental conditions (such as pH, solution conductivity, cell voltage and current density) for color removal, energy consumption, electrode consumption and sludge production [14]. Many researchers discussed the effect of operation parameters such as solution pH, initial

* Corresponding author.

contaminant concentration and electrolyte concentration on the energy consumption and removal efficiency [15–20].

Although there are a lot of literatures about the application and optimization of EC, its industrial application is not yet considered as an established wastewater technology because of the lack of systematic models for reactor scale-up [21,22]. Most of the literatures are using the statistical models for optimization [23–27]. The models about mass transfer and momentum transfer during continuous or batch EC processes were seldom investigated [1,28].

A review of electrocoagulation modeling approaches was made by Hakizimana et al. [29]. Dubrawski et al. [30] developed a numerical model considering electric charge conservation to simulate the potential and current distribution during EC process. A 2D model [31] was established to study the effect of cell geometry and electrode configuration on EC performance. However, only the electric charge conservation is considered. The mass transfer and the electrochemical reaction were not considered. Chen et al. [32] established a one-dimensional electrochemical model to study the effect of electrolysis voltage. Delaire et al. [24] used an existing computational model to investigate the combined effects of pH, Fe dosage rate and O₂ recharge rate on arsenic removal in EC with Fe electrode.

However, these models did not consider the mass transfer and fluid flow. The ionic species concentration of EC channel was considered as uniform distribution. The electrolysis and electrode reaction rate were considered as a constant. Thus, these models are far from perfect to describe the process. A steady-state continuous EC model considering electrochemical reaction, hydrolysis reaction, mass and momentum transfer were established in our previous paper [1]. The generation and mass transfer of ionic species in EC process was discussed.

Bipolar electrode is widely used in electrochemical processes. In electro-coagulation process, the bipolar electrode acts similar to a coagulant releasing system [33]. The Al³⁺ and OH⁻ are released from the same bipolar electrode. The following paper presents a mathematical model simulating EC process with bipolar electrode. The EC with bipolar electrodes (B-EC) and EC with monopolar electrodes (M-EC) are compared. The generation and mass transfer of coagulants released from bipolar electrode surface are modeled. The generation and mass transfer of soluble and insoluble hydroxides are simulated. The effect of mass transfer behavior of coagulants and flocs on the EC performance was discussed. The edge effects of bipolar electrode in B-EC were modeled and studied with the consideration of mass transfer.

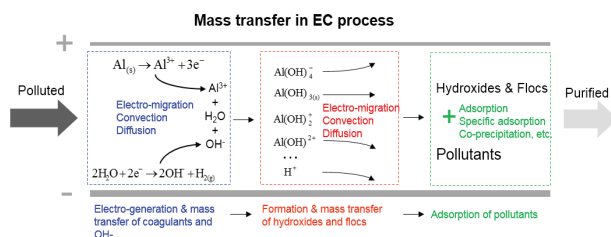


Fig. 1. Mass transfer principles in continuous EC process [1].

2. Mathematical formulations

The structure of continuous EC model is illustrated in Fig. 2. The B-EC is shown in Fig. 2(a). The M-EC is shown in Fig. 2(b). The solution flows into the channel at an initial velocity. In order to avoid inlet's boundary influence on the flow field, an insulation wall with a length of 5 mm was set at the inlet. The forced convection was assumed along the channel. The aluminum electrodes were used. The current density was set as 0–20 A/m². The supporting electrolyte was Na₂SO₄ (10 mol/m³). The residence time was set as 0–1 min. The pH value of the influent solution was set as 7. For B-EC and M-EC, the channel size is 10 × 40 mm. For B-EC, the size of bipolar electrode is 0.5 × 4 mm. There are 15 bipolar electrodes and 10 monopolar electrodes in B-EC.

2.1. Electro-generation of coagulants and OH⁻

During EC with aluminum electrodes, the electro-generated Al³⁺ will react with OH⁻ (originated from cathode surface) to form various aluminum hydroxide products which will finally transform into amorphous Al(OH)_{3(s)}.

The anode reaction is as follows:



Water electrolysis occurs at the cathode:



As the reaction proceeds, passivation film will be produced at the anode surface. The Al³⁺ releasing reaction will be hindered by the passivation. Water will be oxidized to form hydrogen and protons at the anode surface. Also at the condition of high cell voltage, water will be oxidized at the anode surface. The water oxidation reaction is as follows:

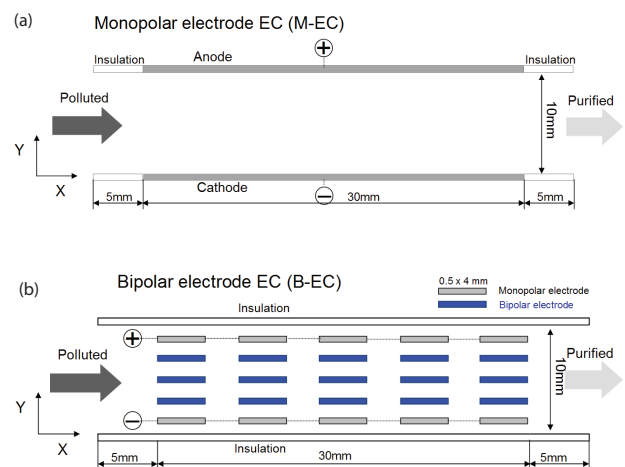
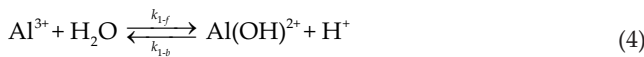


Fig. 2. Illustration of continuous M-EC (a) and B-EC (b) reactor model.

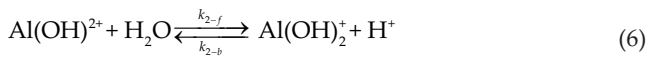
2.2. Formation of soluble and insoluble hydroxides

The electro-generated coagulant Al^{3+} and OH^- will transfer into bulk solution and hydrolyze to monomeric and polymeric hydroxides such as $\text{Al}(\text{OH})^{2+}$, $\text{Al}(\text{OH})_2^+$, $\text{Al}(\text{OH})_{3(s)}$, $\text{Al}(\text{OH})_4^-$, $\text{Al}(\text{OH})_5^{2-}$, $\text{Al}_2(\text{OH})_2^{4+}$, $\text{Al}_6(\text{OH})_{15}^{3+}$, $\text{Al}_7(\text{OH})_{17}^{4+}$, $\text{Al}_8(\text{OH})_{20}^{4+}$, etc. [1,34]. In order to simplify the model, the formation of polymeric hydroxides was not considered. Only the monomeric hydroxides $\text{Al}(\text{OH})^{2+}$, $\text{Al}(\text{OH})_2^+$, $\text{Al}(\text{OH})_{3(s)}$, and $\text{Al}(\text{OH})_4^-$ were considered in this model [1]. The hydrolysis and water dissociation reactions involved were shown below:



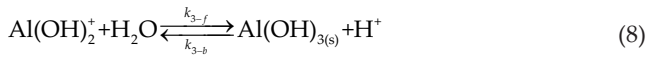
The reaction rate is as follows:

$$r_{\text{hydro},1} = k_{1-f} \cdot c_{\text{Al}^{3+}} - k_{1-b} \cdot c_{\text{Al}(\text{OH})^{2+}} \cdot c_{\text{H}^+} \quad (5)$$



The reaction rate is as follows:

$$r_{\text{hydro},2} = k_{2-f} \cdot c_{\text{Al}(\text{OH})^{2+}} - k_{2-b} \cdot c_{\text{Al}(\text{OH})_2^+} \cdot c_{\text{H}^+} \quad (7)$$



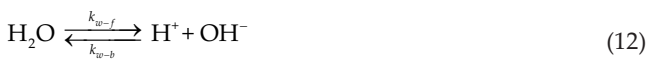
The reaction rate is as follows:

$$r_{\text{hydro},3} = k_{3-f} \cdot c_{\text{Al}(\text{OH})_2^+} - k_{3-b} \cdot c_{\text{Al}(\text{OH})_{3(s)}} \cdot c_{\text{H}^+} \quad (9)$$



The reaction rate is as follows:

$$r_{\text{hydro},4} = k_{4-f} \cdot c_{\text{Al}(\text{OH})_{3(s)}} - k_{4-b} \cdot c_{\text{Al}(\text{OH})_4^-} \cdot c_{\text{H}^+} \quad (11)$$



The reaction rate is as follows:

$$r_w = k_{w-b} (K_w - c_{\text{H}^+} \cdot c_{\text{OH}^-}) \quad (13)$$

where c_i is the concentration of species i ; k is the reaction rate constant.

2.3. Mass transfer of ionic species

2.3.1. Governing equations

The mass transfer flux of species i is given by Nernst–Planck equation [35,36]. There are three types of mass

transport flux in EC channel: diffusion, electro-migration and convection. They are written as $-D_i \nabla c_i$, $Z_i \mu_i c_i (-\nabla \phi)$, and $U c_i$ respectively. The total mass transfer flux of species i is written as follows:

$$N_i = -D_i \nabla c_i + z_i \mu_i c_i (-\nabla \phi) + U c_i \quad (14)$$

where D_i and Z_i are diffusion coefficient and charge number of species i , respectively; ϕ represents electric potential; μ_i is the ionic migration rate and could be deduced from the Nernst–Einstein equation:

$$\mu_i = \frac{D_i F}{RT} \quad (15)$$

where F is the Faraday constant.

U is the flow velocity vector. The fluid flow was modeled with the incompressible Navier–Stokes equation (N–S equation) [1,37].

The equation for mass conservation of species i is as follows:

$$\frac{\partial c_i}{\partial t} + \nabla \cdot N_i = R_i \quad (16)$$

where R_i is the reaction rate of species i .

The reaction rate of species i in bulk solution is as follows:

$$R_i \Big|_{i=\text{Na}^+} = 0 \quad (17)$$

$$R_i \Big|_{i=\text{SO}_4^{2-}} = 0 \quad (18)$$

$$R_i \Big|_{i=\text{Al}^{3+}} = -r_{\text{hydro},1} \quad (19)$$

$$R_i \Big|_{i=\text{Al}(\text{OH})^{2+}} = r_{\text{hydro},1} - r_{\text{hydro},2} \quad (20)$$

$$R_i \Big|_{i=\text{Al}(\text{OH})_2^+} = r_{\text{hydro},2} - r_{\text{hydro},3} \quad (21)$$

$$R_i \Big|_{i=\text{Al}(\text{OH})_{3(s)}} = r_{\text{hydro},3} - r_{\text{hydro},4} \quad (22)$$

$$R_i \Big|_{i=\text{Al}(\text{OH})_4^-} = r_{\text{hydro},4} \quad (23)$$

$$R_i \Big|_{i=\text{H}^+} = r_{\text{hydro},1} + r_{\text{hydro},2} + r_{\text{hydro},3} + r_{\text{hydro},4} + r_w \quad (24)$$

$$R_i \Big|_{i=\text{OH}^-} = r_w \quad (25)$$

The current density is as follows:

$$i = F \sum_{i=1}^n Z_i N_i \quad (26)$$

$$i = F \sum_{i=1}^n (-D_i \nabla c_i - z_i \mu_i c_i \nabla \phi_i) \quad (27)$$

The electro-neutrality equation is as follows:

$$\sum_{i=1}^N Z_i c_i = 0 \quad (28)$$

2.3.2. Boundary conditions

The electrode current density is set as uniform current density. The total current of B-EC and M-EC is same.

$$i = F \sum_{i=1}^n (-D_i \nabla c_i - z_i \mu_i c_i \nabla \phi_i) = i_0 \quad (29)$$

The mass transfer flux of species at anode surface is as follows:

$$N_i \Big|_{i=Al^{3+}} = \frac{i_0}{3F}; \quad N_i \Big|_{i=other\ species} = 0 \quad (30)$$

The current density at cathode surface is set as follows:

$$i = F \sum_{i=1}^n (-D_i \nabla c_i - z_i \mu_i c_i \nabla \phi_i) = -i_0 \quad (31)$$

The mass transfer flux of species at cathode surface is as follows:

$$N_i \Big|_{i=OH^-} = -\frac{i_0}{F}; \quad N_i \Big|_{i=other\ species} = 0 \quad (32)$$

The boundary condition of inlet area is set as follows:

$$c_i \Big|_{i=Na^+} = c_{Na^+,0}; \quad c_i \Big|_{SO_4^{2-}} = c_{SO_4^{2-},0}; \quad c_i \Big|_{i=other\ species} = 0 \quad (33)$$

The potential of inlet boundary is set as reference potential.

$$\phi = 0 \quad (34)$$

It is assumed that all the mass passing through the outlet boundary is convection-dominated.

$$(-D_i \nabla c_i - Z_i \mu_i c_i \nabla \phi) \Big|_{i=all\ species} = 0 \quad (35)$$

Thus, the current density across the outlet boundary is also zero.

$$i = F \sum_{i=1}^n (-D_i \nabla c_i - z_i \mu_i c_i \nabla \phi_i) = 0 \quad (36)$$

The insulation boundary condition is set as follows:

$$N_i \Big|_{i=all\ species} = 0 \quad (37)$$

$$i = F \sum_{i=1}^n (-D_i \nabla c_i - z_i \mu_i c_i \nabla \phi_i) = 0 \quad (38)$$

2.4. Numerical method

The finite element software, COMSOL Multiphysics 3.5A, is used to solve the nonlinear PDEs [35,36]. The two-dimensional EC reactor was meshed by the mesh generator of COMSOL. Quadrilateral elements were used. The method converges when the weighted absolute residual norm is less than 10^{-6} . The stationary segregated nonlinear solver was chosen as the solver. The parameters for the model are shown in Table 1.

3. Results and discussion

3.1. Comparison between B-EC and M-EC

During EC process, the electro-generated coagulant (Fe^{2+} or Al^{3+}) and OH^- will transfer into the bulk solution and undergo further spontaneous hydrolysis reactions to form various monomeric and polymeric hydroxide species, part of which will finally transform into insoluble hydroxide flocs ($Al(OH)_{3(s)}$). These flocs have large surface areas, which are beneficial for a rapid adsorption and pollutant trapping. Thus the generation of the flocs during B-EC and M-EC should be investigated.

For comparison, the B-EC and M-EC were simulated at the same total current density. The current density of the electrode of the M-EC and B-EC is 10 and 3.75 A/m², respectively. At the same total current, the electro-generated coagulant Al^{3+} of bipolar and monopolar electrode structures is equal. The Al^{3+} will hydrolysis with the OH^- generated from cathode to form hydroxide flocs. However, the generated hydroxide flocs are not equal for the bipolar and monopolar electrode structures. A 2D distribution of generated $Al(OH)_{3(s)}$ during B-EC and M-EC at same total current is illustrated in Fig. 3. It could be found that the concentration of generated $Al(OH)_{3(s)}$ flocs in B-EC is much larger than that of M-EC. The amount of generated $Al(OH)_{3(s)}$ flocs differs a lot between B-EC and M-EC.

This could be explained by the mass transfer of ionic species in EC channel. The Al^{3+} hydrolysis reaction rate will increase with the presence of OH^- . Thus, the hydrolysis reaction rate is dependent on the mixture of Al^{3+} and OH^- . There are three types of mass transfer: diffusion, convection and electro-migration. However, only the diffusion and electro-migration at Y-direction could contribute to the mixture of these ions.

During M-EC process, the cation hydroxide species are accumulated on the anode surface area (H^+ controlled area). There is no cation hydroxide ions in the cathode surface (OH^- controlled area) [1]. In other words, the cation Al hydroxide species could not transfer into the OH^- controlled area [1]. The flux of cation hydroxide ions is also near in the

Table 1
Values of parameters for modeling

Parameter	Value	Reference
Diffusion coefficient of Na^+ , D_1	$1.333 \times 10^{-9} \text{ m}^2 \text{ s}^{-1}$	[35,36]
Diffusion coefficient of SO_4^{2-} , D_2	$1.08 \times 10^{-9} \text{ m}^2 \text{ s}^{-1}$	[35,36]
Diffusion coefficient of H^+ , D_H	$9.308 \times 10^{-9} \text{ m}^2 \text{ s}^{-1}$	[35,36]
Diffusion coefficient of OH^- , D_{OH}	$5.280 \times 10^{-9} \text{ m}^2 \text{ s}^{-1}$	[35,36]
Diffusion coefficient of Al^{3+} , $D_{\text{Al}^{3+}}$	$1.011 \times 10^{-9} \text{ m}^2 \text{ s}^{-1}$	
Water density, ρ	$1,000 \text{ kg m}^{-3}$	
Water dynamic viscosity, η	0.001 Pa s	
Reverse direction reaction rate constant of water dissociation, k_{w-b}	$1.5 \times 10^{-8} \text{ m}^3 \text{ mol}^{-1} \text{ s}^{-1}$	
Ion-product constant of free water, K_w	1×10^{-8}	
Reaction rate constant of hydrolysis reaction of Al^{3+} (forward), k_{1-f}	$4.2 \times 10^4 \text{ s}^{-1}$	[38]
Reaction rate constant of first hydrolysis reaction of Al^{3+} (backward), k_{1-b}	$4.2 \times 10^6 \text{ m}^3 \text{ mol}^{-1} \text{ s}^{-1}$	[38]
Value of hydrolysis constant (reaction 3), pK_1	4.95	[38,39]
Value of hydrolysis constant (reaction 5), pK_2	5.60	[38,39]
Value of hydrolysis constant (reaction 7), pK_3	6.70	[38,39]
Value of hydrolysis constant (reaction 9), pK_4	5.60	[38,39]
Retention time in EC channel, R_t	1 min	
Influent pH value	7	
Influent electrolyte concentration, Na_2SO_4	10 mol m^{-3}	
Current density of electrode of M-EC	10 A m^{-2}	
Current density of bipolar electrode of B-EC	3.75 A m^{-2}	

OH^- controlled area. Thus the $\text{Al(OH)}_{3(s)}$ will be generated in the area where the Al^{3+} and OH^- meet with each other. It could be found that the $\text{Al(OH)}_{3(s)}$ is generated in the extremely narrow area, which is located in the middle of EC channel. It can be found in Fig. 3.

During B-EC process, every bipolar electrode has anode and cathode side. Al^{3+} and OH^- are released from anode and cathode of the same electrode. The distance between the anode and cathode is much closer. In Y-direction, the Al^{3+} and OH^- will electro-migrate in a very short range to meet with each other. The result is that the reaction rate of Al^{3+} hydrolysis in channel during B-EC is larger than that of M-EC. When compared with EC with monopolar electrode, the bipolar electrode structure (or porous electrode structure) improves the mass transfer of coagulants and OH^- originated from anode and cathode, respectively. Also the bipolar electrode structure improves the depth of Al^{3+} hydrolysis reaction. A 2D distribution of generated ionic hydroxide species is illustrated in Fig. 4. In M-EC, almost all of the Al-containing species are in the form of ionic Al hydroxide species. In B-EC, most of the electro-generated Al^{3+} ions transform into $\text{Al(OH)}_{3(s)}$ and the concentration of ionic Al hydroxide species is very low.

Also, another fact must be mentioned is that the $\text{Al(OH)}_{3(s)}$ produced in B-EC process is distributed very uniformly. The reason is that during B-EC, the Al^{3+} and OH^- are well distributed in every bipolar electrode channel. During M-EC process, the $\text{Al(OH)}_{3(s)}$ is produced in a very narrow area. During B-EC and M-EC, the concentration profile of $\text{Al(OH)}_{3(s)}$ at the cross-section of the outlet area is illustrated in Fig. 5. During continuous M-EC, the flocs with very narrow distribution are not beneficial for the mixture of pollutant and flocs. The low

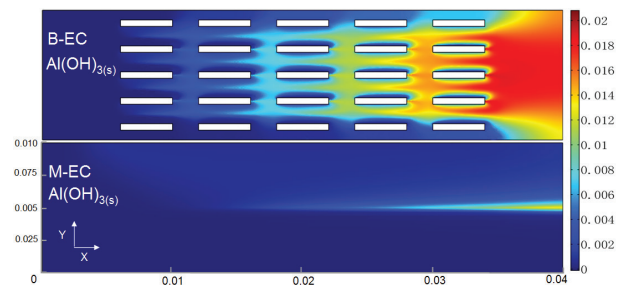


Fig. 3. 2D distribution of generated $\text{Al(OH)}_{3(s)}$ flocs during B-EC and M-EC, mol/m^3 .

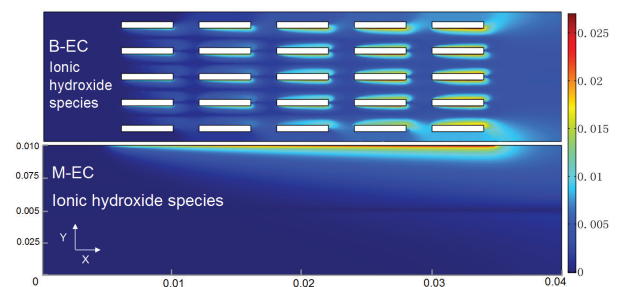


Fig. 4. 2D distribution of generated ionic hydroxide species during B-EC and M-EC, mol/m^3 .

mixture of pollutant and flocs could be overcome by the stirring or aeration. Thus, during continuous or batch M-EC process the stirring or aeration is necessary.

In EC process, OH^- is generated by the cathode reaction. The H^+ is produced by the Al^{3+} hydrolysis reaction near the anode surface [1]. The produced H^+ and OH^- will control the

hydrolysis reaction rate, which is very sensitive to the pH condition. Higher H^+ or OH^- concentration is not suitable for the formulation of Al hydroxide flocs. During B-EC process, the H^+ and OH^- are generated at the anode and cathode surface of every bipolar electrode. The concentration of H^+ and OH^- generated in B-EC and M-EC is illustrated in Fig. 6.

Under the same total current, the current density of B-EC is lower than that of M-EC. The total production of Al^{3+} and OH^- during B-EC and M-EC is same. The concentration of electro-generated Al^{3+} and OH^- and generated H^+ is lower in B-EC. The lower concentration of H^+ and OH^- is suitable for the formation of Al hydroxide flocs [34]. This is another reason why the B-EC has a higher flocs production.

3.2. Edge effects of bipolar electrode during B-EC process

During B-EC process, the bipolar electrodes act similar to a coagulant releasing system. The bipolar electrode structure may have electrode edge effect which is common in electrochemical reactors.

The Al^{3+} and OH^- are released from anode and cathode surface of the same bipolar electrode. The mixture of Al^{3+} and OH^- are mainly implemented by the electro-migration

in Y-direction (perpendicular to electrode surface). In electrochemical process, the currents are carried by the ions under electro-migration and diffusion. Most of the current are transferred by the ions under electro-migration. Thus the magnitude and direction of current could be an important parameter for the mixture of these ions.

In the electrochemistry process, for the electrode with high length/width ratio, the edge effect of electrode could be neglected [1]. However, in B-EC process, the length/width ratio is not high. The edge effects of electrode should be mentioned. The edge effects of electrode could be found in the current distribution figure (Fig. 7). The color shows the value of current density. The arrow shows the direction of currents. The current density in bulk area (A) is uniform (same magnitude and direction). It could be considered as uniform electric field. However, at the area B and C, the magnitude and direction of

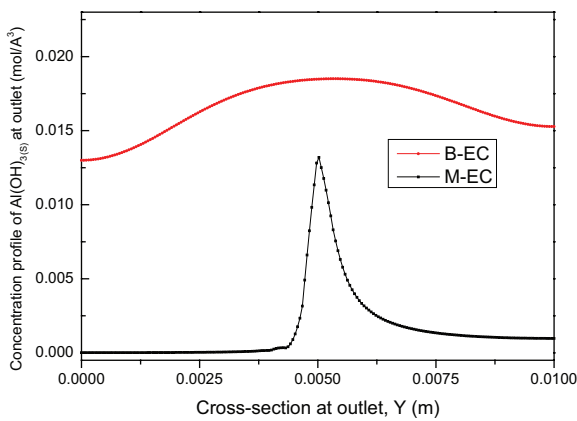


Fig. 5. Concentration profile of $Al(OH)_{3(s)}$ at the cross-section of the outlet area.

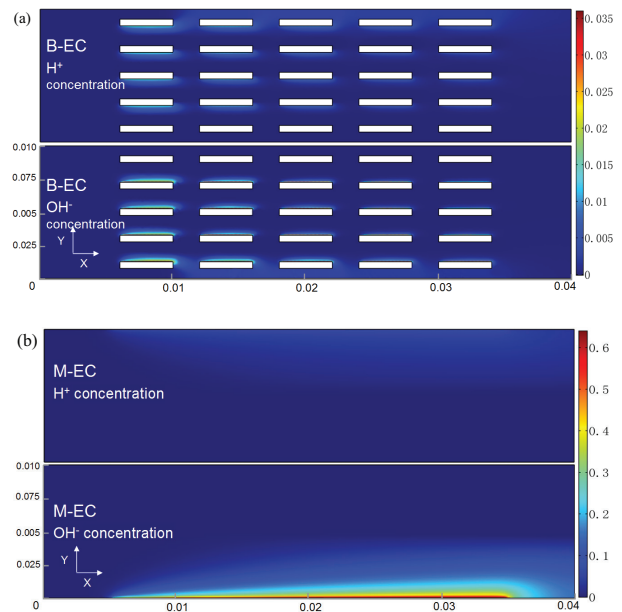


Fig. 6. 2D distribution of generated H^+ and OH^- during B-EC (a) and M-EC (b), mol/m^3 .

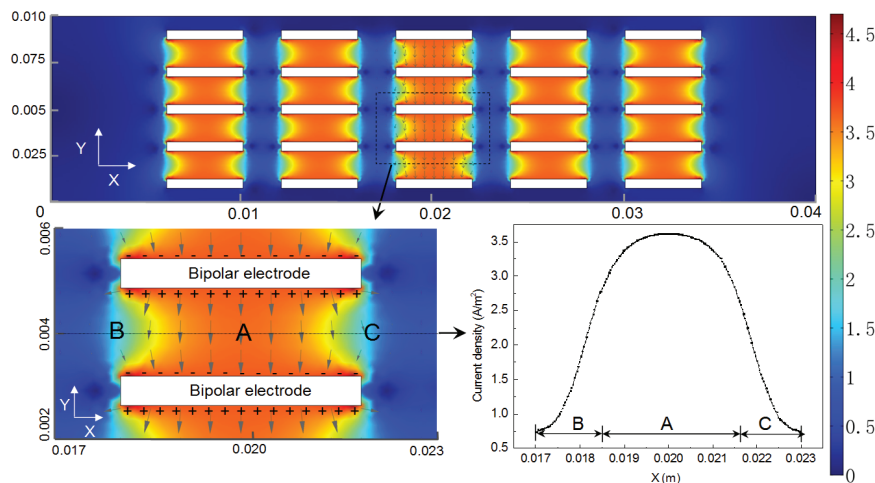


Fig. 7. Current density distribution in B-EC, A/m^2 .

currents change with the position. The current decreases from the center area (A) of bipolar electrode channel to the edge area (B and C). The profile of current density at the channel center of bipolar electrode is illustrated in Fig. 7.

With the consideration of current distribution, the edge effects of bipolar electrode may be significant. However, from the aspect of the mixture of the coagulants and the hydroxide species, the edge effects of bipolar electrode in EC process could be neglected. The concentration of cation (area C1) and anion (area C2) hydroxide species is not negligible (Fig. 8). In these edge areas (C1 and C2), the direction of current is not perpendicular to the streamline. In edge area C1 and C2, the electro-migration in Y-direction (perpendicular to the electrode surface) will also make the cation and anion hydroxide species transfer into the bulk channel. The electro-migration in X-direction could not contribute to the mixture of coagulants. It will accelerate the convection in X-direction. In edge area, the electro-migration could also contribute to the mixture of the ions. Thus, during the bipolar electro-coagulation process, the edge effect of bipolar electrode could be neglected.

3.3. Limitations of current EC model

During the continuous EC process, the hydrogen will be generated from cathode surface. The flocs will be generated in the EC channel. Thus there are three phases (solution, gas and floc phase) in the EC channel. In this work, the multiphase flow was not considered in this model. The multiphase flow will take an important effect on the mass transfer. The interaction between mass transfer and multiphase flow should be considered in the future work.

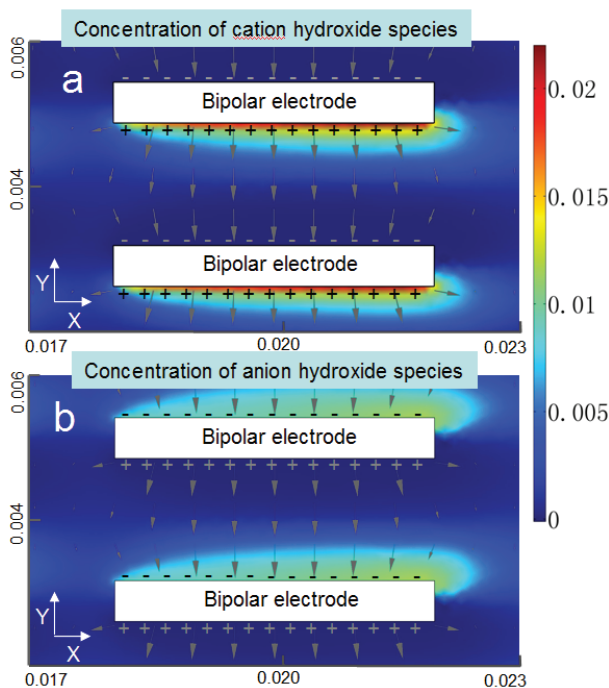


Fig. 8. 2D distribution of cation (a) and anion (b) hydroxide species around bipolar electrode, mol/m³.

4. Conclusions

The continuous electrocoagulation (EC) with bipolar electrode was modeled and simulated. The generation and mass transfer of coagulants released from bipolar electrode surface are modeled. The generation and mass transfer of soluble and insoluble hydroxides are simulated.

The electrocoagulation with bipolar electrode (B-EC) was compared with the electrocoagulation with monopolar electrode (M-EC), which is commonly used. Under the same total current, the B-EC has a much higher flocs production than that of M-EC. This is due to the fact that the bipolar electrode structure has a better mass transfer which leads to a better mixture of generated coagulants and OH⁻ during B-EC. During M-EC, the hydroxide flocs are generated in an extremely narrow area. The steric hindrance effect will lead to lower adsorption ability of the flocs. However, during B-EC, the hydroxide flocs are uniformly generated and distributed in the channel. This is beneficial for the formation of hydroxide flocs.

The concentration of produced H⁺ and OH⁻ is much lower in B-EC. The lower concentration of H⁺ and OH⁻ is suitable for the formation of Al hydrate flocs. This is another reason why the B-EC has a higher flocs production. Also low OH⁻ concentration will lower the probability of electrode erosion.

The edge effects of bipolar electrode in B-EC were modeled and studied. The edge effects were discussed with the consideration of mass transfer. The magnitude and direction of the current change and decrease from the bulk channel to the edge area. In the edge areas, the concentration of cation and anion hydroxide species is not negligible. In these areas, the electro-migration will also make the cation and anion hydroxide species transfer into the bulk channel. Thus, in edge area, the electro-migration could also contribute to the mixture of the ions. The edge effect of bipolar electrode in EC process could be neglected. The EC process with bipolar electrodes shows a better mass transfer performance than that with monopolar electrodes.

Acknowledgments

This study was funded by the National Natural Science Foundation of China (NSFC No. 51208233 and 51603094) and Postgraduate Research & Practice Innovation Program of Jiangsu Province.

References

- [1] J. Lu, Z.R. Wang, X.Y. Ma, Q. Tang, Y. Li, Modeling of the electrocoagulation process: a study on the mass transfer of electrolysis and hydrolysis products, *Chem. Eng. Sci.*, 165 (2017) 165–176.
- [2] M. Vepsäläinen, M. Pulliainen, M. Sillanpää, Effect of electrochemical cell structure on natural organic matter (NOM) removal from surface water through electrocoagulation (EC), *Sep. Purif. Technol.*, 99 (2012) 20–27.
- [3] A. Akyol, Treatment of paint manufacturing wastewater by electrocoagulation, *Desalination*, 285 (2012) 91–99.
- [4] J. Lu, Z.R. Wang, Y.L. Liu, Q. Tang, Removal of Cr ions from aqueous solution using batch electrocoagulation: Cr removal mechanism and utilization rate of in situ generated metal ions, *Process Saf. Environ. Prot.*, 104 (2016) 436–443.
- [5] D. Lakshmanan, D.A. Clifford, G. Samanta, Ferric and ferric ion generation during iron electrocoagulation, *Environ. Sci. Technol.*, 43 (2009) 3853–3859.

- [6] U. Tezcan Un, A. Savas Kopalal, U. Bakir Ogutveren, Fluoride removal from water and wastewater with a batch cylindrical electrode using electrocoagulation, *Chem. Eng. J.*, 223 (2013) 110–115.
- [7] T. Harif, M. Khai, A. Adin, Electrocoagulation versus chemical coagulation: coagulation/flocculation mechanisms and resulting floc characteristics, *Water Res.*, 46 (2012) 3177–3188.
- [8] D. Lakshmanan, D.A. Clifford, G. Samanta, Comparative study of arsenic removal by iron using electrocoagulation and chemical coagulation, *Water Res.*, 44 (2010) 5641–5652.
- [9] J. Lu, Q. Tang, Z.R. Wang, C. Xu, S.L. Lin, A study on continuous and batch electrocoagulation process for fluoride removal, *Desal. Wat. Treat.*, 57 (2016) 28417–28425.
- [10] J. Lu, Y. Li, M.X. Yin, X.Y. Ma, S.L. Lin, Removing heavy metal ions with continuous aluminum electrocoagulation: a study on back mixing and utilization rate of electro-generated Al ions, *Chem. Eng. J.*, 267 (2015) 86–92.
- [11] S. Ahmadzadeha, A. Asadipour, M. Yoosefian, M. Dolatabadie, Improved electrocoagulation process using chitosan for efficient removal of cefazolin antibiotic from hospital wastewater through sweep flocculation and adsorption: kinetic and isotherm study, *Desal. Wat. Treat.*, 92 (2017) 160–171.
- [12] S. Ahmadzadeh, A. Asadipour, M. Pournamdari, B. Behnam, H.R. Rahimi, M. Dolatabadi, Removal of ciprofloxacin from hospital wastewater using electrocoagulation technique by aluminum electrode; optimization and modelling through response surface methodology, *Process Saf. Environ. Prot.*, 109 (2017) 538–547.
- [13] M. Yoosefian, S. Ahmadzadeh, M. Aghasi, M. Dolatabadi, Optimization of electrocoagulation process for efficient removal of ciprofloxacin antibiotic using iron electrode: kinetic and isotherm studies of adsorption, *J. Mol. Liq.*, 225 (2017) 544–553.
- [14] K.W. Pi, Q. Xiao, H.Q. Zhang, M. Xia, A.R. Gerson, Decolorization of synthetic Methyl Orange wastewater by electrocoagulation with periodic reversal of electrodes and optimization by RSM, *Process Saf. Environ.*, 92 (2014) 796–806.
- [15] N. Drouiche, S. Aoudj, H. Lounici, M. Drouiche, T. Ouslimane, N. Ghaffour, Fluoride removal from pretreated photovoltaic wastewater by electrocoagulation: an investigation of the effect of operational parameters, *Procedia Eng.*, 33 (2012) 385–391.
- [16] E. Bazrafshan, K.A. Ownagh, A.H. Mahvi, Application of electrocoagulation process using iron and aluminum electrodes for fluoride removal from aqueous environment, *J. Chem.*, 9 (2012) 2297–2308.
- [17] M.M. Emamjomeh, M. Sivakumar, Fluoride removal by a continuous flow electrocoagulation reactor, *J. Environ. Manage.*, 90 (2009) 1204–1212.
- [18] Y. Tian, W. He, X. Zhu, W. Yang, N. Ren, B.E. Logan, Energy efficient electrocoagulation using an air-breathing cathode to remove nutrients from wastewater, *Chem. Eng. J.*, 292 (2016) 308–314.
- [19] Y. Si, G. Li, F. Zhang, Energy-efficient oxidation and removal of arsenite from groundwater using air-cathode iron electrocoagulation, *Environ. Sci. Technol.*, 2 (2016) 71–75.
- [20] J.H. Kim, H.A. Maitlo, J.Y. Park, Treatment of synthetic arsenate wastewater with iron-air fuel cell electrocoagulation to supply drinking water and electricity in remote areas, *Water Res.*, 115 (2017) 278–286.
- [21] P. Song, Z. Yang, G. Zeng, X. Yang, H. Xu, L. Wang, R. Xu, W. Xiong, K. Ahmad, Electrocoagulation treatment of arsenic in wastewaters: a comprehensive review, *Chem. Eng. J.*, 317 (2017) 707–725.
- [22] P.V. Nidheesh, T.S.A. Singh, Arsenic removal by electrocoagulation process: recent trends and removal mechanism, *Chemosphere*, 181 (2017) 418–432.
- [23] N. Balasubramanian, T. Kojima, C. Srinivasakannan, Arsenic removal through electrocoagulation: kinetic and statistical modeling, *Chem. Eng. J.*, 155 (2009) 76–82.
- [24] C. Delaire, S. Amrose, M. Zhang, J. Hake, A. Gadgil, How do operating conditions affect As(III) removal by iron electrocoagulation?, *Water Res.*, 112 (2017) 185–194.
- [25] B. Yang, Y. Han, G. Yu, Q. Zhuo, S. Deng, J. Wu, P. Zhang, Efficient removal of perfluoroalkyl acids (PFAAs) from aqueous solution by electrocoagulation using iron electrode, *Chem. Eng. J.*, 303 (2016) 384–390.
- [26] Z. Ma, Y. Yang, Y. Jiang, B. Xi, T. Yang, X. Peng, X. Lian, K. Yan, H. Liu, Enhanced degradation of 2,4-dinitrotoluene in groundwater by persulfate activated using iron-carbon micro-electrolysis, *Chem. Eng. J.*, 311 (2017) 183–190.
- [27] K.S. Hashim, A. Shaw, R. Al Khaddar, M.O. Pedrola, D. Phipps, Iron removal, energy consumption and operating cost of electrocoagulation of drinking water using a new flow column reactor, *J. Environ. Manage.*, 189 (2017) 98–108.
- [28] L. Li, C.M.v. Genuchten, S.E.A. Addy, J. Yao, N. Gao, A.J. Gadgil, Modeling As(III) oxidation and removal with iron electrocoagulation in groundwater, *Environ. Sci. Technol.*, 46 (2012) 12038–12045.
- [29] J.N. Hakizimana, B. Gourich, M. Chafi, Y. Stiriba, C. Vial, P. Drogui, J. Naja, Electrocoagulation process in water treatment: a review of electrocoagulation modeling approaches, *Desalination*, 404 (2017) 1–21.
- [30] K.L. Dubrawski, C. Du, M. Mohseni, General potential-current model and validation for electrocoagulation, *Electrochim. Acta*, 129 (2014) 187–195.
- [31] A. Vazquez, I. Rodriguez, I. Lazaro, Primary potential and current density distribution analysis: a first approach for designing electrocoagulation reactors, *Chem. Eng. J.*, 179 (2012) 253–261.
- [32] X. Chen, G. Chen, P.L. Yue, Investigation on the electrolysis voltage of electrocoagulation, *Chem. Eng. Sci.*, 57 (2002) 2449–2455.
- [33] Z. Qi, S. You, N. Ren, Wireless electrocoagulation in water treatment based on bipolar electrochemistry, *Electrochim. Acta*, 229 (2017) 96–101.
- [34] M. Mechelhoff, G.H. Kelsall, N.J.D. Graham, Electrochemical behaviour of aluminium in electrocoagulation processes, *Chem. Eng. Sci.*, 95 (2013) 301–312.
- [35] J. Lu, Y.X. Wang, J. Zhu, Numerical simulation of the electrodeionization (EDI) process accounting for water dissociation, *Electrochim. Acta*, 55 (2010) 2673–2686.
- [36] J. Lu, Y.X. Wang, Y.Y. Lu, G.L. Wang, L. Kong, J. Zhu, Numerical simulation of the electrodeionization (EDI) process for producing ultrapure water, *Electrochim. Acta*, 55 (2010) 7188–7198.
- [37] J. Lu, X.Y. Ma, Y.X. Wang, Numerical simulation of the electrodeionization (EDI) process with layered resin bed for deeply separating salt ions, *Desal. Wat. Treat.*, 57 (2015) 10546–10559.
- [38] L.P. Holmes, D.L. Cole, E.M. Eyring, Kinetics of aluminum ion hydrolysis in dilute solutions, *J. Phys. Chem.*, 72 (1968) 301–304.
- [39] J.M. Duan, J. Gregory, Coagulation by hydrolysing metal salts, *Adv. Colloid Interface Sci.*, 100–102 (2003) 475–502.